SAND2006-4399C

Effects of inertia on wall deposition in particle-laden turbulent channel flow

John R. Schmidt[1], Jost O. L. Wendt[2]
Department of Chemical and Environmental Engineering
University of Arizona, Tucson, AZ 85721
and
Alan R. Kerstein
Combustion Research Facility,
Sandia National Laboratories, Livermore, California 94551-0969

(Received

The slow relaxation of high-inertia particles to statistical equilibrium with flow fluctuations in turbulence is known to affect deposition rates, but satisfactory modeling of this process has not yet been achieved. A simple analysis of the transient response of high-inertia particles predicts that the deposition rate in the far field of a turbulent channel flow obeys a -2/3 power-law dependence on the wall-normalized particle relaxation time τ_p^+. The analysis also implies a near-field deposition regime that is less sensitive to τ_p^+, consistent with experiments and numerical simulations that indicate weaker dependence. The gradual onset of the asymptotic regime suggests that careful attention to slow transients is important for valid interpretation of such results.

To illustrate these and other features of high-inertia deposition, a computationally efficient stochastic model is used to investigate both the near-field and far-field behavior. The model that is employed is a two-phase flow (one-way coupling) extension of One Dimensional Turbulence (ODT). The novel features developed for this application of ODT are described in detail. To broaden the perspective, ODT channel-flow deposition results are presented and interpreted for a wide range of τ_p^+ values spanning several deposition regimes.

PACS numbers: 47.55.Kf, 47.27.-i, 47.60.+i

[1] Corresponding author, jschmidt@arl.army.mil, Current affiliation: Army Research Laboratory, Aberdeen Proving Ground, Maryland 21005
[2] Current affiliation: Department of Chemical Engineering, University of Utah, Salt Lake City, UT 84112

I. INTRODUCTION

Predicting particle deposition from turbulent flows is essential for industrial and environmental applications and remains challenging even under idealized assumptions. The focus here is particle deposition from turbulent channel flow based on one-way coupling and Stokes drag, in some cases incorporating a particle-Reynolds-number correction. Gravitational effects are omitted. Although the phenomenology of particle transport and dispersion in boundary layers is understood,[1] predictive modeling of particle deposition based on the governing conservation laws is the focus of ongoing research.[2-4] Here it is proposed that deposition of high-inertia particles is governed by a previously unrecognized scaling, although the physical basis for this scaling is implicit in previous work.[2,4]

The regime of interest (high inertia, downstream of near-field transients) is difficult to investigate experimentally and is marginally accessible using 3D simulations. It is studied here in two ways, by heuristic scaling analysis and by developing and applying a two-phase generalization of a 1D stochastic turbulence simulation model. The scaling analysis identifies the novel deposition regime. The 1D simulations reproduce the predicted scaling. To relate this observation to previous work, the model is applied to a wide range of conditions (moderate as well as high particle inertia, near-field as well as far-field regimes, different Re values) and is compared to pertinent experimental and 3D simulation results.

Pertinent phenomenology is summarized in Sec. II. The new high-inertia scaling is introduced in Sec. III. The 1D numerical model is formulated in Sec. IV. Results obtained using the numerical model are presented and discussed in Secs. V and VI.

II. DEPOSITION REGIMES

The rate of particle deposition from turbulent boundary layers is generally characterized by a wall-normalized deposition velocity V_d^+, whose dependence on the particle Stokes number τ_p^+, expressed in wall units, is the main property of interest. The deposition velocity V_d is obtained by dividing particle deposition flux by bulk-averaged particle concentration. Then $V_d^+ = V_d/u_\tau$, where u_τ is the friction velocity, and $\tau_p^+ = \tau_p u_\tau^2/\nu$, where τ_p is the particle aerodynamic time constant and ν is the kinematic viscosity.

Measurements of the dependence of V_d^+ on τ_p^+ exhibit three distinct regimes termed the diffusional-deposition, diffusional-impaction, and inertia-moderated regimes, with transitions at $\tau_p^+ = 0.3$ and 30 respectively. The present focus is the high-inertia regime corresponding to τ_p^+ far greater than the latter transition, although the diffusional-impaction regime is also considered in order to support the conclusions drawn about high-inertia behavior.

In the inertia-moderated regime, measurements up to τ_p^+ of order 10^3 suggest a barely perceptible (relative to experimental uncertainty) decline of V_d^+ with increasing τ_p^+.[2,5] The behavior in this τ_p^+ range (and at small τ_p^+) is reproduced by Eulerian closure-type models.[2,4] It is recognized that this decline is due to the decreasing effectiveness of turbulence in inducing lateral deflections of particles as particle inertia increases.

Large-eddy simulation (LES) of pipe-flow deposition extending to higher τ_p^+ values (up to 10^4) suggests[6] an acceleration of the declining trend for $\tau_p^+ > 10^3$. There does not appear to be subsequent discussion of this observation in the literature, leaving open the question of whether the aforementioned models capture this effect.

A physical basis for accelerating decline is identified here using a straightforward scaling analysis. A computational model is then used to demonstrate the predicted behavior. It is inferred that this ostensibly large-τ_p^+ regime has significant implications with regard to the low-

τ_p^+ end of the inertia-moderated deposition regime. The reason is that the onset of the asymptotic behavior occurs only after a long transient relaxation period. Previously reported weak τ_p^+ dependence seen at large τ_p^+ [2,7,8] might be partially the result of observation during the initial transient rather than the ultimate statistically steady evolution. This suggests that further computational and experimental study might be needed in order to distinguish asymptotic behavior from initial transients. Previous analysis by Graham[9] has analogous implications, albeit without addressing the particular regimes and evolution mechanisms considered here.

III. ANALYSIS OF HIGH-INERTIA DEPOSITION

A. Scaling analysis

To derive the parameter dependencies of V_d^+ in the limit of high particle inertia, the turbulent channel flow is characterized by three velocity scales: the bulk velocity u_b, a turbulent fluctuation amplitude u', and the friction velocity u_τ. The other governing quantities are the channel half-height h, the particle response time τ_p, and the kinematic viscosity ν. h/ν times each of the respective velocity scales defines bulk, turbulent, and friction Reynolds numbers Re_b, Re', and Re_τ.

The three velocity scales parameterize the lateral (y) variation of flow structure. In terms of this parameterization, it will be seen that this lateral structure affects V_d^+ through parameters that depend only on fluid flow, and that the dependence of V_d^+ on τ_p is insensitive to these details, and in particular is valid for both channel and pipe flow.

The fluid flow is assumed to be statistically steady. Various particle initial conditions are considered, but the results for these cases differ only in minor details, so the case considered first is the one that is simplest to analyze. Namely, it is assumed that particles traveling at streamwise velocity u_b are introduced, with zero lateral or spanwise velocity, at the flow mid-plane. Accordingly, while a particle is in the core-flow region its streamwise velocity is of order u_b.

High turbulence intensity (based on any of the defined Reynolds numbers) is assumed, so the near-wall region where the mean fluid velocity $\langle u(y) \rangle$ obeys $\langle u(y) \rangle << h$ is small compared to h. For simplicity, Stokes drag is assumed with no particle-Reynolds-number correction.

For large τ_p, particle acceleration by individual turbulent eddies is slight, so the streamwise particle slip $S_U = U - u$ is typically of order u', where u' is taken to be the large-eddy velocity. The lateral slip $S_V = V - v$ is of the same order. Spanwise slip is immaterial under the stated assumptions and therefore is not considered.

The turbulence integral scale is of order h, so the large-eddy time scale is $T \sim h/u'$. Because S_U is of order u', the particle eddy-crossing time is also of order T. Based on Stokes drag, the particle velocity change in a given direction while crossing an eddy scales as ST/τ_p, where S is the corresponding slip component, S_U or S_V, both scaling as u'. The particle velocity change caused by a large-eddy traversal is then $\Delta U \sim \Delta V \sim h/\tau_p$.

During a time interval $t >> T$, a particle is subject to order t/T independent velocity increments due to these eddy effects. This corresponds to diffusive growth in time of the velocity scale V (and analogously for U, but consideration of U is set aside temporarily), obeying the scaling $V(t) \sim \Delta V \, (t/T)^{1/2} \sim (h/\tau_p) \, (t/T)^{1/2}$. This can be expressed as $dV^2/dt \sim D$, where the velocity diffusion coefficient D obeys $D \sim u'^2 T/\tau_p^2$. This is valid if t is short compared to the time required for $V(t)$ to reach statistical equilibrium with respect to the velocity impulses ΔV that drive the growth of V. This is verified in Sec. III.B for the t range of interest.

The deposition time t_d is estimated to be the time t at which $\int_0^t V(t')\, dt' = h/2$. This gives $(t_d^3/T)^{1/2} \sim \tau_p$ and thus

$$t_d \sim (T\tau_p^2)^{1/3}. \tag{1}$$

Assuming that the deposition velocity V_d scales as h/t_d (which is justified in Sec. III.B), it then obeys

$$V_d \sim (h/T)(T/\tau_p)^{2/3}. \quad (2)$$

To express this relation in wall units, it is divided by u_τ, giving $V_d^+ = (h/u_\tau)(Tt_\tau^2)^{-1/3}\ (\tau_p^+)^{-2/3}$, where $t_\tau = \nu/u_\tau^2$ and $\tau_p^+ = \tau_p/t_\tau$. This identifies the τ_p^+ dependence of V_d^+. Substitution of $T \sim h/u'$ and rearrangement gives

$$V_d^+ \sim (\mathrm{Re}_\tau \mathrm{Re}')^{1/3}\ (\tau_p^+)^{-2/3}. \quad (3)$$

The relation $u' \sim u_\tau$ would reduce this to $V_d^+ = \mathrm{Re}_\tau^{2/3}(\tau_p^+)^{-2/3}$, but this is not assumed due to experimental[10] and computational[11] evidence of deviations of u' from wall scaling. Wall scaling of u′ can nevertheless be viewed as a bounding case, another obvious bound being $u' \sim u_b$. The latter scaling implies $V_d^+ = (\mathrm{Re}_\tau\ \mathrm{Re}_b)^{1/3}(\tau_p^+)^{-2/3}$. This can be simplified using the Blasius resistance formula, long regarded as empirical but recently derived from a more fundamental perspective.[12] The Blasius formula, $f \sim \mathrm{Re}_b^{-1/4}$, where the friction factor f scales as $(\mathrm{Re}_\tau/\mathrm{Re}_b)^2$, implies $\mathrm{Re}_b \sim \mathrm{Re}_\tau^{8/7}$ and thus $V_d^+ = \mathrm{Re}_\tau^{5/7}(\tau_p^+)^{-2/3}$. The situation can be summarized by the relation

$$V_d^+ \sim \mathrm{Re}_\tau^{\,p}\ (\tau_p^+)^{-2/3}, \quad (4)$$

where $2/3 < p < 5/7$ and therefore $p \approx 0.7$.

B. Initial conditions, transients, and equilibration

Based on Eq. (1), $t_d/\tau_p \sim (T/\tau_p)^{1/3}$, which is much less than unity in the limit of large τ_p. The time required for V to transition from transient growth to equilibration is much longer than this. This transition occurs when V^2 reaches its equilibrium value determined by $dV^2/dt \sim D - V^2/\tau_p = 0$. Here, the sink term V^2/τ_p omitted from the derivation of Eq. (2) is included. This gives the familiar[3] equilibrium result

$$V^2 \sim D\ \tau_p \sim u'^2\ T/\tau_p. \quad (5)$$

Until the onset of equilibration, $V^2(t) \sim Dt$, showing that the elapsed time until equilibration is τ_p, which is much larger than the estimated deposition time t_d. The particle lateral velocity at time t_d

obeys $V(t_d) \sim (h/T)\,(T/\tau_p)\,(\tau_p/T)^{1/3} \sim u'\,(T/\tau_p)^{2/3}$, which is smaller than the equilibrium value by the factor $(T/\tau_p)^{1/6}$. These estimates indicate that the transient analysis is self-consistent.

Analogous considerations indicate that, if mean streamwise slip is negligible, then perturbations of the particle streamwise velocity U are of likewise order $u'\,(T/\tau_p)^{2/3}$ and therefore have negligible effect on particle streamwise displacement during the time interval t_d. If the streamwise slip is nonzero initially, e.g., for the case of particles that are initially motionless ($U(0) = V(0) = 0$), then the particle U velocity relaxes to the mean flow velocity (order u_b) during a time interval τ_p. Because $t_d << \tau_p$, this indicates that the particle U velocity remains much smaller than u_b throughout the deposition process.

This raises the question of the dependence of the scaling of V_d on initial conditions. First, the dependence of V_d on U is considered, retaining the V initial condition $V(0) = 0$. The assumption $V_d \sim h/t_d$ is examined in this regard. Namely, the Lagrangian perspective of the foregoing analysis is compared to the Eulerian definition of V_d as the particle deposition flux F divided by the particle number density n. Consider particles in a flow moving downstream at speed U and depositing on channel walls at a rate that scales as n/t_d. Particles contained in a notional control volume $A\,\Delta x$ moving downstream at speed U, where A is the channel cross-sectional area and Δx is a given streamwise increment, deposit over a streamwise interval of order $X = Ut_d$, here assuming $\Delta x << X$. Therefore, the number of particles depositing from this control volume per unit surface area of the channel is of order $n\,A\,\Delta x/(\sigma X)$, where sigma is the channel surface area per unit streamwise distance. During time t_d, the number of such control volumes traversing the streamwise interval X is $X/\Delta x$, so the total number of particles deposited per unit surface area during time t_d is of order nA/σ. Dividing by t_d and n gives $V_d = F/n \sim A/(\sigma t_d)$. In a channel, A/σ is the half-height h, yielding the assumed scaling $V_d \sim h/t_d$.

The analysis predicated on this scaling involves U only in the determination of the particle eddy-crossing time h/S_U, where $S_U \sim u'$ provided that U is no larger than order u'. If instead $U >> u'$, then h/U is substituted for T throughout the analysis, corresponding the multiplication of the right-hand side of Eq. (4) by $(UT/h)^{1/3} \sim (U/u')^{1/3}$. Because the change of U is slight during the time interval t_d, $U(0)$ can be substituted for U in this term. The situation is summarized by the relation

$$V_d^+ \sim \max(1,[U(0)/u']^{1/3}) \, \mathrm{Re}_\tau^{\,p} (\tau_p^+)^{-2/3}. \tag{6}$$

Next, nonzero $V(0)$ is considered. Owing to the smallness of the deviations from ballistic particle trajectories for large τ_p/T, the deposition time t_d for $V(0) \neq 0$ is $h/V(0)$ unless $V(0)$ is small enough so that $h/V(0)$ is larger than t_d given by Eq. (1). Thus, Eq. (1) is an upper bound on the deposition time, which can be much smaller for nonzero $V(0)$.

More generally, assume a distribution of particle $V(0)$ values. In general, $h/V(0)$ will be smaller than t_d for most particles, so most of the deposition will be ballistic in character and more rapid than predicted by Eq. (6). However, the (generally small) fraction of particles for which $V(0) < h/t_d$ deposit by the non-equilibrium mechanism analyzed here, and accordingly their deposition rate is governed by Eq. (6).

The small fraction of particles obeying Eq. (6) in this scenario indicates that for large τ_p/T, deposition is predominantly ballistic and thus is governed primarily by initial conditions. This indicates that high-inertia deposition for the conditions considered (Stokes drag, zero gravity), is primarily a transient, case-specific process, and that phenomenology of a more general nature arises only as a far-field (downstream) asymptote. Implications with regard to the interpretation of measurements and simulation results are considered in Sec. V.C.

It is assumed in the analysis that particles are introduced at the channel mid-plane, but the far-field analysis is unchanged if a more general initial spatial distribution is assumed. Only the

small fraction of particles introduced at a distance from the wall that is much less than h will deposit more rapidly than the analysis predicts. The near-field transient deposition due to nonzero $V(0)$ may be strongly affected by the initial spatial distribution. This dependence is likewise considered in Sec. V.C.

In Eq. (6), the τ_p^+ term follows from the diffusive scaling governing the transient evolution of the magnitude of $V(t)$. In contrast, the Re_τ term arises from an idealized picture of turbulent channel flow structure. For example, u' is taken to be a characteristic velocity scale of the entire flow, omitting the consideration that turbulent velocity fluctuations are concentrated primarily in the vicinity of the wall, peaking sharply before falling to zero at the wall. Therefore the Re_τ dependence is less firmly established than the τ_p^+ dependence.

The analysis highlights the non-equilibrium character of particle response to turbulent fluctuations in the regime of interest. Nevertheless, the equilibrium condition, Eq. (5), is adopted in closure-type modeling of particle deposition in turbulent channel flow.[2,3] The deficiency of this assumption is recognized and a compensatory modification has been attempted, but the closure framework does not readily accommodate a fundamentally sound representation of non-equilibrium.[3,4] Reflecting this, closure modeling predicts less rapid decrease of V_d^+ with increasing τ_p^+ than is indicated by Eq. (6). The milder dependence is found to be consistent with experimental and numerical simulation results. However, these results reflect case-specific near-field transient phenomena rather than the far-field asymptote, as shown in Sec. V.C. Therefore, the consistency of these results with closure model predictions is not as clear a validation of model assumptions as it may appear.

IV. STOCHASTIC SIMULATION OF INERTIAL PARTICLES IN TURBULENT FLOW

A. Motivation

The analysis of Sec. III suggests that high-inertia deposition is challenging to investigate both experimentally and computationally. The slow relaxation of transients requires a large experimental apparatus in order to observe the far-field asymptote, as emphasized by Graham.[9] Likewise, it requires large spatial domains in numerical simulations (or long run times, in the more usual temporally developing configuration). The non-equilibrium character of high-inertia deposition is not readily accommodated in closure models. Given these difficulties, the question arises as to whether there is any practical way to study this regime apart from the heuristic scaling analysis of Sec. III.

One of the authors has developed a cost-effective method for simulating turbulence and its coupling to other processes using a modeling strategy based on reduction of spatial dimensionality. A 1D spatial representation is employed. It has been shown that a stochastic simulation model formulated in 1D provides a representation of turbulence phenomenology that is useful in many respects.[13,14]

This approach, denoted One-Dimensional Turbulence (ODT), is generalized here for simulation of inertial particles in turbulence. It is shown that this formulation not only captures the relevant physics of turbulent particle deposition, but also provides both the fidelity and efficiency needed to investigate high-inertia deposition as well as other deposition regimes. Computed results support the analysis of Sec. III and its implications and provide other relevant insights.

B. Turbulence model

The ODT formulation previously used to simulate turbulent channel flow[15] is adopted here. Because it is described and validated in the cited reference and other published work,[14] the description here is brief and is specific to the present application.

It is instructive to introduce for comparison a simple boundary-layer representation of fully developed channel flow based on eddy-viscosity modeling,

$$\frac{\partial u}{\partial t} = \frac{\partial}{\partial y}\left(\nu_e \frac{\partial u}{\partial y} \right) + \nu \frac{\partial^2 u}{\partial y^2} - \frac{1}{\rho}\frac{dp}{dx} \qquad (7)$$

where t is time (denoted t_f in Sec. IV.C to distinguish it from a particle time coordinate), y is the lateral coordinate, ν is kinematic viscosity, ν_e is the modeled eddy viscosity, ρ is density, and dp/dx is an imposed mean pressure gradient in the streamwise direction. ν_e is typically assumed to be a time-invariant function of y, yielding a steady state formulation in which the time derivative vanishes.

Suppose instead that ν_e is time varying. This allows the possibility of unsteady evolution governed by Eq. (7) rather than the usual steady-state formulation in which $u(y)$ represents the mean velocity profile. This generalization would require modeling of $\nu_e(y,t)$. One way to obtain a closed formulation would be to express ν_e as some prescribed function of y and $u(y',t)$. Here y' designates the set of all lateral locations within the channel, $0 < y' < 2h$, corresponding to a nonlocal closure of ν_e. This reduces to a more familiar local closure if the argument y' is restricted to the value y.

Consideration of the advantages and limitations of such a formulation serves to motivate the present approach. Equation (7) with the suggested closure is reminiscent of unsteady RANS and

in this sense is a qualitative step beyond steady-state modeling. For given y, dependence of ν_e on the flow state at all lateral offsets $l = y' - y$ offers the possibility of dependence of turbulent transport on a range of structure scales l at each y rather than a unique functional dependence $l(y)$, as is assumed in mixing-length formulations.

Practical realization of these conceptual advantages would require a closure of the stated form that drives sustained unsteadiness of Eq. (7) rather than inducing relaxation to steady state. Moreover, such unsteady feedback through the closure formulation must be demonstrably physical in its construction and outcome. These requirements are difficult to satisfy because $-\nu_e$ represents an ensemble averaged flux of u divided by an ensemble average of du/dy, even though the evolution equation is nominally unsteady. Models of advective transport that scale diffusively represents the cumulative effect of numerous statistically distinct (if not fully independent) advection motions, and hence do not capture unsteadiness at time scales too short for diffusive scaling to apply locally.

Accordingly, individual advective motions over a distance l are better represented as fluid displacements than as gradient-driven fluxes. Indeed, fluid displacement is the primitive element of Prandtl's mixing-length phenomenology, although through averaging it ultimately leads to diffusive representation of turbulent transport.

In 2D or 3D, displacement corresponds to time integration of the advection term $\boldsymbol{u} \cdot \nabla(\ )$. Except for trivial rigid-body displacement, there is no continuous-in-time 1D representation of advection that satisfies basic requirements (conservation laws of constant-property flow, no creation of spontaneous singularities). Accordingly, advection is represented in 1D as a time sequence of instantaneous displacements, each formulated to represent the outcome of a notional turbulent eddy motion. Formally, the outcome of simulated evolution from time 0 to time t can then be expressed as

$$u(y,t) = T[t_n,t]\, E(\boldsymbol{p}_n) \cdots T[t_i,t_{i+1}]\, E(\boldsymbol{p}_i)\, T[t_{i-1},t_i] \cdots E(\boldsymbol{p}_2)\, T[t_1,t_2]\, E(\boldsymbol{p}_1)\, T[0,t_1]\, u(y,0), \qquad (8)$$

where capital letters represent operators. $T[t_{i-1},t_i]$ represents time advancement of the operand $u(y,t_{i-1})$ from t_{i-1} to t_i, governed by Eq. (7) with the eddy-viscosity term omitted. $E(\boldsymbol{p}_i)$ is an 'eddy event,' an instantaneous transformation of the operand $u(y,t_i)$ representing a turbulent eddy motion. $\boldsymbol{p}_i$ represents the set (vector) of randomly sampled quantities determining the exact form of the ith transformation. n is the number of eddy events during $[0,t]$, t_i is the time of occurrence of the ith event for $i > 0$, and $t_0 = 0$. The epochs t_i, the quantities $\boldsymbol{p}_i$, and n are random variables evaluated during each simulated realization by a sampling procedure. The sampling rules embody the principal physical content of the model.

In higher dimensions, numerical advancement of the exact governing equations can likewise be represented by Eq. (8), but with different interpretations. u is replaced by the vector velocity field $\boldsymbol{u}$ and its spatial argument is a point in d-dimensional space. T now represents evolution by the exact equations, but with the advection operator omitted, and E represents advancement by the advection operator. $t_i - t_{i-1}$ is now the advancement time step (typically uniform). Equation (8) then encodes a conventional split-operator advancement scheme, involving no random sampling and therefore giving a unique final state for a given initial state. If the advection step is Lagrangian (perhaps followed by remapping to an Eulerian mesh), then it corresponds to a collection of fluid displacements, analogous to the meaning of the operator E in 1D.

In ODT, the eddy event represents the outcome of the physical process of eddy turnover, so epochs t_i are sampled based on physical modeling considerations rather than numerical considerations. (In numerical implementation of ODT, the operation $T[t_{i-1},t_i]$ is implemented by choosing the numerically appropriate time step for advancement from t_{i-1} to t_i.)

In Appendix A, details of the specification of an eddy event and the procedures for sampling event epochs and parameters are presented. Features that are relevant to the incorporation of inertial particles are as follows. First, the eddy parameters $\boldsymbol{p}$ are a lower boundary y_o and a size l, determining the upper boundary y_o+l. Second, event occurrences are random samples from an

event rate distribution that assigns a time scale $\tau(y_o, l; t)$, analogous to an eddy turnover time, to each possible event based on the flow state at time t. Third, the operation E specifies displacements $y \rightarrow \{y_1', y_2', y_3'\}$ for y within the interval $[y_o, y_o+l]$, where each of the three images y_j' is within that interval. In fact, the images occupy successive thirds of the interval, thus filling the interval. Each image is a threefold compression of the original interval, except that the central (second) image is inverted (spatially flipped). There is no displacement at y values outside the interval $[y_o, y_o+l]$. Graphical illustrations and extensive discussions of this 'triplet-map' operation are presented elsewhere.[13,16] (Also see Appendix A.)

Two other pertinent features of the ODT formulation used here are noted. First, it evolves the y profiles of all three velocity components u, v, and w, although a version that evolves only the u profile would suffice for present purposes. (This choice is motivated by prior validation of the three-component version for channel-flow modeling.) For v and w, the time-advancement equation (T process; see Appendix A for details) is the same as for u except that the pressure term is omitted. Second, different ODT formulations involve different numbers of free parameters; the version used here involves three. Here, these parameters are fixed at previously determined values,[15] as explained in Appendix A. Incorporation of inertial particles (Sec. IV.C) introduces one additional adjustable parameter.

C. Inertial particle submodel

Because the turbulent flow model evolves all three velocity components, an obvious way to incorporate inertial particles is to evolve particle velocities U, V, and W by substituting the ODT-specified fluid velocities $u(Y,t)$, $v(Y,t)$, and $w(Y,t)$, into the particle drag law, where Y is the particle location at time t. Time integration of U, V, and W advances the particle location (X,Y,Z). Because the particle is confined to the ODT domain, the ODT fluid state is deemed to represent

the lateral profiles of the fluid velocity components at the (X,Z) location at which the particle currently resides. Flow time advancement on the ODT domain thus represents the spatial as well as temporal variability of the fluid velocity seen by the particle. This implies a relationship between particle and flow advancement that is explained shortly.

This approach has been implemented and results have been compared to measurements and simulations of various particle statistics in turbulent channel flow.[17] Although this approach is found to be successful in some respects, it is not pursued here because it violates a key property of particle advection; namely, that in the zero-inertia (marker particle) limit, a particle should remain co-located with the fluid element that contains it initially.

Ostensibly, a marker particle advected by a specified fluid velocity satisfies this requirement, but in ODT the evolving velocity component v does not advect fluid. In fact, as noted at the end of Sec. IV.B, for channel-flow simulation it suffices to evolve only the streamwise component u. This reflects the fact that eddy events rather than the usual advective operator are the mechanism of fluid advection along the ODT domain.

For consistency with the marker particle limit, the particle-fluid coupling must therefore allow the instantaneous displacement of particles by eddy events. Because this coupling is based on a drag law that must be time integrated to obtain its effect on particle displacement, it is evident that some method must be devised to account for the finite time duration of turbulent motions.

The needed ingredients are available within ODT. The specific goal is to interpret a fluid displacement $y \rightarrow y_j'$ as fluid motion at some specified velocity that is constant (for simplicity) for some specified time interval that is here termed the eddy lifetime. In Sec. IV.B it is noted that eddy event selection involves the specification of an eddy time scale τ. Because this is the only time scale available in ODT to represent eddy properties, the eddy lifetime t_E is modeled as $\beta\tau$, where β is an adjustable parameter, the only new parameter required in the ODT particle

representation. To obtain the specified lateral displacement from motion at constant lateral velocity during the time interval t_E, the velocity must then be

$$v_E = (y_j' - y) / t_E. \qquad (9)$$

It is now straightforward in principle to specify the particle-eddy interaction, although some details require care. The present approach has much in common with particle-eddy interaction sub-models that have been used in RANS formulations,[18] although the implementation is different in several respects. To keep the development general, it is not specialized to a particular form of the drag law until Sec. IV.D.

Assume that a particle is located at (X,Y,Z) and has velocity components (U,V,W) at the time $t = t_i$ when the ith eddy event occurs and assume that $y = Y$ is within the eddy interval $[y_o, y_o+l]$. Then the particle location Y is mapped by the eddy event to each of three locations y_j'. Unlike a fluid element, which is divisible, a particle can be displaced to only one location. Therefore one of the locations y_j' is selected by randomly sampling one of the three, each with probability 1/3. The selected location is denoted y', here dropping the subscript. Each sampling is independent for each particle within the eddy event and for each eddy event encountered by a particle during the simulation. It has been shown that this procedure yields a physically sound representation of the evolution of a particle ensemble in turbulence.[19]

Note that while y' is the location to which fluid at Y is mapped, the particle is not necessarily mapped to y' unless it is a marker particle. The procedure determining the final location Y', as well as the other descriptors of the particle state at the conclusion of the particle-eddy interaction, is now considered.

During the particle-eddy interaction, whose time duration is denoted t_I, the lateral velocity of the fluid initially at $y = Y$ is modeled according to Eq. (9). It is not strictly accurate to infer that the particle initially at $y = Y$ is subject to this fluid velocity throughout the interaction period because the trajectory of an inertial particle will deviate from the trajectory of the fluid initially at

Y. Nevertheless, the modeling assumption is adopted that v_E is the fluid velocity seen by the particle throughout the interaction period. Alternate assumptions introduce additional complexity with no clear gain in physical fidelity.

The duration of the interaction is denoted t_I rather than t_E because the particle may cease to interact with the eddy before the eddy reaches the end of its life. This cessation is due to the emergence of the particle from the spatial region occupied by the eddy. In ODT, the y interval occupied by the eddy, denoted $[y_o,y_o+l]$, is specified by the eddy sampling procedure. The parameter l can be used to infer the streamwise and spanwise as well as lateral extent of the eddy, and the streamwise velocity profile u within the eddy interval at the time of eddy occurrence can be used to infer its rate of streamwise displacement. These geometrical properties, in conjunction with the particle trajectory solution described shortly, are used to determine the first occurrence, if any, of particle emergence from the spatial region occupied by the eddy. If this occurs before elapsed time t_E, then t_I is set equal to the time of this first occurrence, otherwise t_I is set equal to t_E. This feature of the model is important when particle-eddy interaction is dominated by trajectory-crossing effects, as in the case of high-inertia particles subject to gravitation. However, these effects are not important for the cases considered here, so details of the determination of t_I, reported elsewhere,[20] are not repeated here.

Based on the foregoing considerations, the particle drag law is time integrated, based on the fluid state $(u(Y,t_i),v_E,w(Y,t_i))$, to advance the particle from its initial state (X,Y,Z,U,V,W) to its state (X',Y',Z',U',V',W') at time t_I, where this advancement contributes to the determination of t_I as noted. Note that the streamwise and spanwise, as well as lateral, fluid velocity components are evaluated at the initial particle location, again because there is no straightforward alternate assumption.

Although this advancement specifies new values of all particle coordinates and velocity components, only the lateral particle location and velocity are modified by the particle-eddy

interaction. This is because evolution of the other coordinates and components are adequately represented by particle advancement during the time intervals between eddy events. (Recall that the special treatment of lateral advancement is for the specific purpose of assuring that eddy events result in appropriate marker-particle behavior in the zero-inertia limit.) Thus, the updated state variables (X',Z',U',W') obtained from drag-law integration play no role in subsequent advancement. These variables are time advanced during particle-eddy interaction for the sole purpose of evaluating t_I by following the particle trajectory to determine whether emergence from the eddy occurs during the eddy lifetime, and if so when.

The nominal particle state at the end of particle-eddy interaction is thus (X,Y',Z,U,V',W). The primed variables reflect advancement for a time interval t_I starting from the state at time t_i, but the unprimed variables correspond to the state at t_i.

ODT eddies are instantaneous, so the state immediately after an eddy corresponds to time t_i. Time advancement subsequent to particle-eddy interaction (particle T process) thus begins at time t_i, implying a period of advancement in physical time that overlaps the time advancement implemented during particle-eddy interaction.

The duplication of particle advancement implied by this overlap is corrected as follows. Particle-eddy interaction as described thus far determines new values (Y',V') of the particle lateral location and velocity by integrating the drag law for a time interval t_I starting from the initial state (Y,V) and holding the fluid velocity fixed at $(u(Y,t_i),v_E,w(Y,t_i))$. A second drag-law integration is introduced, over the same time interval and starting from the same initial state, except that the fluid velocity is held fixed at $(u(Y,t_i),0,w(Y,t_i))$. The values of the particle lateral variables upon completion of this integration are denoted (Y_0',V_0'). The physical state of the particle upon completion of particle-eddy interaction is then taken to be (X,Y'',Z,U,V'',W), where $Y'' = Y + Y' - Y_0'$ and $V'' = V + V' - V_0'$.

The rationale for this procedure is illustrated by considering the limiting cases of infinite-inertia and zero-inertia particles. For infinite particle inertia, the value of v_E has no effect on particle advancement, so $Y' = Y_0'$, giving $Y'' = Y$. Likewise, $V'' = V$. Thus, the eddy interaction has no effect on the particle and it continues on its ballistic (linear) trajectory during subsequent advancement. (Particle evolution between eddy interactions is explained shortly.) This is the physically correct result. For zero particle inertia, $Y' = y'$, $Y_0' = Y$, and thus $Y'' = y'$. Likewise, $V' = v_E$, $V_0' = 0$, so $V'' = v_E$. The result for Y'' is the physically correct marker-particle behavior. The result for V'' is immaterial because the marker particle immediately relaxes to zero velocity.

It is seen that the subtraction procedure is suitable for the limiting cases and can be expected to provide a reasonable interpolation between these cases for finite-inertia particles. Representative case studies verify this.[20] Conceptually, the procedure evaluates the net effect of the interaction on the particle relative to particle evolution if the eddy had not occurred. By defining the particle-eddy interaction based on this difference, it is consistent to implement the outcome of the interaction instantaneously at time t_i despite the fact that it is computed by means of time integration from t_i to t_{i+} t_I.

For some configurations, e.g., particles moving rapidly in the ODT domain direction y, the instantaneous nature of eddy events might cause particles to encounter eddy events much less often than they would encounter physical eddies of finite time duration. Accurate modeling of such configurations requires eddy events as perceived by particles to have finite durations in the physical time coordinate as well as in the internal time coordinate introduced to model particle-eddy interactions. A formulation of this type has been developed[20] but it is not used here because it is considerably more elaborate than the present formulation, which is suitable for the flow regimes considered here.

The evolution of a particle within an ODT simulation can be represented schematically by Eq. (8), but with different interpretation of symbols than for fluid evolution. In Eq. (8), u is replaced

by the particle state (X,Y,Z,U,V,W), evaluated at time t on the left-hand side and at time 0 on the right-hand side. E is now interpreted as a particle-eddy interaction. Description of the model is now completed by specifying the particle advancement T that occurs during the time intervals between these interactions.

This process consists of time advancement of the particle state (X,Y,Z,U,V,W), evaluated at time t, based on the drag law with fluid velocity $(u[Y(t),t],0,w[Y(t),t])$. In the drag law used for this advancement, the lateral component of fluid velocity is set equal to zero in order to maintain consistency with the marker-particle limit. In ODT as implemented here, fluid is advected laterally only by eddy events. As noted earlier, the ODT v velocity profile is an auxiliary variable that does not directly govern lateral fluid advection.

One consequence of this formulation is that V converges toward zero during the T process. This is an artifact of the separation of the time coordinate into finite intervals with zero lateral motion, alternating with instantaneous lateral displacements. As a result, the particle V value upon the initiation of a particle-eddy interaction may be unrealistically low, and tests indicate that this is indeed typical at moderate τ_p^+. Therefore the initial V value in the time integration performed to evaluate the particle-eddy interaction is taken to be not the current value, but the value V'' obtained as the outcome of the most recent eddy interaction involving the given particle.

Through the evaluation of t_I, the particle-eddy interaction has been formulated to take account of trajectory-crossing effects, although these effects are unimportant in the flow regimes considered here. Trajectory-crossing effects are likewise incorporated into the T process. Explicit treatment of these effects during the T process is needed because the particle streamwise advancement $dX = U\,dt$ implies trajectory crossing if $dX \neq dx$ where dx is the streamwise fluid advancement $u(Y,t)\,dt$ at the particle location. Particle advancement from t to $t + dt$ subject to drag influence should reflect both flow temporal evolution from t to $t + dt$ and particle traversal of a streamwise interval $|dX - dx|$ of the flow. The contribution of streamwise traversal is

modeled by interpreting the simulated flow evolution on the 1D domain as spatial evolution based on the relation $dx = u_b\, dt_f$, where t_f denotes the time coordinate of the simulated flow evolution. Advancement dt of the particle time coordinate t then corresponds to flow temporal advancement by the same increment dt plus an additional advancement $|dX - dx| / u_b$ intended to represent the difference between the flow states on lateral lines of sight separated by a streamwise distance $|dX - dx|$. This gives

$$dt_f = \left[1 + \frac{|U(t) - u(Y,t)|}{u_b}\right] dt \qquad (10)$$

The second term in the square brackets is a contribution to flow temporal evolution that is adopted here as a model of the difference between flow states at locations separated by a streamwise distance $|dX - dx|$ at a given instant. This model is subject to verification, but present results do not test this model because the contribution of the second term is minor for the flow regimes considered here. Future applications of this formulation to cases involving more consequential streamwise trajectory-crossing effects will test Eq. (10), which for present purposes is an incidental feature of the model.

D. Simulation of deposition in channel flow

Because one-way coupling of particles to the flow is assumed here, the flow simulation is unaffected by the introduction of particles if t_f is taken to be the time variable for system advancement, with Eq. (10) then determining the particle advancement in terms of its time variable t, which is distinct for each particle. On this basis, turbulent channel flow simulation is implemented as in Schmidt et al.[15] using the same ODT parameter values (Appendix A) as in that study. The flow configuration is fully specified by the quantity Re_τ.

Before particles are introduced, the flow simulation is run until it is statistically steady. At a given instant, particles are introduced. In some cases, the initial velocity of each particle is chosen to match the local fluid velocity. The initial lateral distribution of particles is spatially uniform unless noted otherwise. Specifically, the flow evolves on a uniform mesh, and one particle is introduced in the center of each mesh cell. The coarsest meshes have order 10^3 cells; much finer meshes are also used.

Particles are assumed to be spherical. When a particle reaches a lateral location Y that is within one radius of a wall, it is deemed to deposit on the wall and disappears from the simulation. Although particle radii are finite for consistency with comparison cases, they are small enough in all instances so that finite-size effects (relative to the limit of zero radius with τ_p^+ fixed) are negligible. Particles can overlap and pass through each other, i.e., there is no particle-particle interaction, so the simulation can be run at arbitrary particle volume fraction and still represent dilute conditions.

The number of simulated realizations and run time per realization were chosen for various cases so that the number of steady-state particle depositions per plotted V_d^+ value ranged from a minimum of order 10^2 at low inertia to order 10^6 in the vicinity of $\tau_p^+ = 100$, then declining to order 10^4 at high inertia. In the log-log plots of V_d^+ versus τ_p^+ that are shown in Sec. V, the uncertainty of the results is in all instances smaller than the symbol size.

Not all deposition events are included in the determination of V_d^+. Time-resolved deposition statistics, discussed in Sec. V.C, indicate transient relaxation that is especially significant at large τ_p^+. Therefore V_d^+ is determined on the basis of depositions during the period of statistically steady deposition following transient relaxation. The duration of data gathering was predetermined to keep enough particles in the flow to keep the simulation cost-effective.

The model can accommodate drag laws of various degrees of complexity. Here, particle motion is governed by

$$\frac{d\boldsymbol{S}}{dt} = \left(\boldsymbol{s} - \boldsymbol{S}\right)\frac{f}{\tau_p}, \tag{11}$$

$$\frac{d\boldsymbol{X}}{dt} = \boldsymbol{S}\ , \tag{12}$$

$$\tau_p = \frac{2\rho_p r^2}{9\mu}, \tag{13}$$

$$f = \begin{cases} 1 \\ 1 + 0.15\,\mathrm{Re}_p{}^{0.687}, \end{cases} \tag{14}$$

$$\mathrm{Re}_p = \frac{\rho_f r\left|\boldsymbol{s} - \boldsymbol{S}\right|}{\mu}\ , \tag{15}$$

where μ is the fluid viscosity, ρ is density (subscript indicates particle or fluid), r is particle radius, and $\boldsymbol{s}$ and $\boldsymbol{S}$ are fluid and particle velocities, respectively. $f = 1$ corresponds to Stokes drag and the lower expression for f incorporates an empirical correction.[21]

As explained in Sec. IV.C, the model quantities corresponding to the components of $\boldsymbol{s}$ in Eq. (11) depend on whether the particle is being advanced during particle-eddy interaction or during the T process, and if the former, on whether it is the first or second drag-law integration during the interaction. This explains the use of a notation in Eqs. (11)-(15) that does not indicate how $\boldsymbol{s}$ and $\boldsymbol{S}$ are defined in terms of model variables. When the corrected f is used, Eq. (15) is evaluated based on $\boldsymbol{s} = (u,v,w)$ and $\boldsymbol{S} = (U,V,W)$ in all instances. Thus, the ODT v velocity contributes to particle advancement when Eq. (15) is used, but not otherwise (see Sec. IV.C).

During flow evolution, triplet maps are applied to velocity profiles discretized on the mesh, so the maps are implemented numerically as permutations of the discrete values, thus automatically satisfying the conservation properties of the model, which is defined mathematically as spatially continuous. Particle kinematics requires finer spatial resolution near walls than flow evolution. Therefore it is advantageous to exploit the Lagrangian representation of particles by using the

continuum definition of the triplet map, Eq. (A3), to evaluate the fluid displacements that determine fluid velocities seen by particles during particle evolution.

V. RESULTS

A. Parameter assignment

The relation $t_E = \beta\tau$ that defines the eddy lifetime in the particle-eddy interaction submodel introduces the free parameter β. It is adjusted to give the best agreement between ODT deposition simulations and a direct numerical simulation (DNS) of channel-flow deposition.[22] As in the DNS, Stokes drag is used in the ODT simulation. $Re_\tau = 125$ in the DNS, but the ODT comparison case is $Re_\tau = 180$ because the high-Re phenomenology implicit in ODT model assumptions becomes marginally valid at $Re_\tau = 180$ and problematic at lower Re_τ.[15] Re_τ sensitivities presented in Sec. V.B indicate that the difference between the DNS and ODT Re_τ values should not noticeably impact the comparison.

The best agreement is obtained for $\beta = 0.3$, which is used in all subsequent ODT simulations. For this β value, the comparison to the DNS data is shown in Fig. 1. It should be noted that the DNS results are subject to considerable statistical uncertainty; in particular, the lowest data point is based on a single deposition event.

B. Stokes-number dependence of deposition

Although the present focus is deposition at large τ_p^+, it is useful to consider smaller τ_p^+ values as well, both for parameter evaluation (as in Sec. V.A) and to provide a general context for interpretation of model results. Model results for the complete range of τ_p^+ values considered here are shown in Fig. 2 for the same conditions (Stokes drag, $Re_\tau = 180$, $\beta = 0.3$) as in Fig. 1.

Also shown are selected comparison cases, although only qualitative comparison is possible due to the differences between model assumptions and the physics governing these cases.

At small τ_p^+, model results suggest an approach to quadratic dependence of V_d^+ on τ_p^+. A heuristic interpretation of this dependence is presented in Appendix B.

Low-inertia deposition based on Stokes drag is considered here solely for comparison of model processes and other physical pictures of deposition (see Appendix B). Stokes drag is inaccurate at low inertia, as indicated by the comparison between low-inertia model results and DNS results[7] for Re_τ = 125 in Fig. 2. The drag law used in this DNS study includes the Cunningham slip factor, Brownian motion force, Saffman lift, and wall effects on both drag and lift, none of which are included in the present model formulation (although they can be incorporated and will be included in future work).

In this regard, it is fortuitous that the low-inertia measurements[5] shown in Fig. 2 approach the quadratic dependence. The experiment, involving droplet deposition in tubes, was subject to the effects represented in the DNS plus other complications, such as droplet shape distortion and polydispersity, which can plausibly account for the differences between the DNS and experimental results.[7]

Nevertheless, the overall increase of V_d^+ with increasing inertia, followed by leveling (not seen in the DNS data, but an eventual necessity due to the boundedness of V_d^+) is well understood.[2] The low-inertia trend reflects the role of inertia in enabling particles to cross fluid streamlines, as is required for deposition when effects of finite particle radius are negligible. The resulting increase of deposition with increasing inertia saturates when the deposition becomes nearly ballistic and hence relatively insensitive to further increase of inertia.

In Sec. III, analysis of high-inertia deposition indicates that the ballistic mechanism is a near-field transient that is followed by relaxation to a less effective mechanism, resulting in $(\tau_p^+)^{-2/3}$ dependence of V_d^+. The high-inertia results in Fig. 2 are consistent with the interpretation that the

measurements reported in Liu and Agarwal[5] correspond to the near-field ballistic regime and model results correspond to the far-field regime. Additional evidence supporting this interpretation is examined in Sec. V.C.

Also shown in Fig. 2 are measurements[23] that have been interpreted[24] as a decreasing trend following an empirical -1/2 power law. It is noted in passing that the predicted -2/3 high-inertia far-field scaling is an equally good statistical inference, but the aforementioned experimental complications preclude physical inference based on this observation. A mild decreasing trend can also be discerned in the measurements of Liu and Agarwal.[5] As noted in Sec. III.B, models based on lateral equilibration of particle motions, or small corrections thereto, reproduce this trend but not on the basis of a physically sound representation of high-inertia deposition.

The model results in Fig. 2 correspond to a single, moderate value of Re_τ. Sensitivity to Re_τ is shown in Fig. 3. There is noticeable sensitivity at moderate inertia, though not enough either to alter the physical picture or to raise concern about the applicability of the results for $Re_\tau = 180$. The only other apparent sensitivity is at very high inertia. There, the results suggest that $Re_\tau = 180$ may be below the onset of strong turbulence limiting behavior. The results at higher Re_τ show better overall conformance with the -2/3 scaling, but in contrast to the Re_τ dependence in Eq. (4), they indicate at most slight Re_τ dependence at high inertia. As noted in Sec. III, the Re_τ dependence in Eq. (4) relies on stronger assumptions than are required to derive the τ_p^+ dependence.

C. High-inertia deposition

Additional results are presented that elucidate the transient features of high-inertia deposition. In Fig. 4, LES results[8] for $Re_\tau = 180$ are plotted along with results shown in Fig. 2. The LES results exhibit decreasing τ_p^+ sensitivity, consistent with measurements, suggesting eventual

leveling or possible decline. Also shown are model results for cases configured to be quantitatively comparable to the LES cases.

The drag law used in the LES includes the drag correction shown in Eq. (14), so it is included in the corresponding model cases. Also, for these comparisons, the particle initial conditions are the same as in the LES (uniform spatial distribution, particle velocities equal to fluid velocities), and the model is run for the same duration in wall time as the LES, with all particle depositions counted in the determination of V_d^+. In the LES and in the corresponding model cases, Re_τ = 180. (Both the model and LES results indicate insensitivity of deposition to Re_τ at the τ_p^+ values of interest.) This model configuration is also run at $\tau_p^+ = 50$ for comparison to the plotted DNS result at this τ_p^+ value.

Figure 4 shows that the two changes (the drag law and the time interval of data collection) relative to the baseline model results account for almost all of the discrepancy between the LES and baseline model results, and likewise improve the agreement with DNS at $\tau_p^+ = 50$. The effect of the data collection period is further elaborated in Fig. 5, in which the DNS and LES V_d^+ values are compared to model results for time-resolved deposition. Model results indicate that the time variation of V_d^+ during the data-collection period for each comparison case exceeds the differences between the model results and the comparison LES or DNS results that are shown in Fig. 4.

Beyond the LES data-collection period, the model results indicate relaxation to statistically steady deposition with V_d^+ values slightly higher than the baseline (Stokes-drag) values, confirming that the departure from baseline results that is evident in Fig. 4 is mostly due to the difference between near-field transient and far-field statistically steady deposition. Figure 5 indicates the reversal from deposition increasing to deposition decreasing with increasing inertia as the transient relaxes. This behavior is likewise obtained for higher τ_p^+ values.

Recall that statistical steadiness does not necessarily imply equilibration of particle velocities relative to turbulent motions. In fact, the analysis of Sec. III indicates that such equilibration does not occur during the deposition process at very large τ_p^+.

Further illustrations of the distinction between transient and statistically steady deposition are provided in Figs. 5 and 6. For a case that is identical to the $\tau_p^+ = 200$ model case of Fig. 5 except that particles initially have zero velocity and are uniformly distributed within a y interval [-0.6h, 0.6h] relative to the channel mid-plane, Fig. 5 shows an early period of negligible deposition followed by convergence to the $\tau_p^+ = 200$ model case with zero initial slip and spatially uniform initial conditions. This convergence occurs before statistically steady deposition is attained, but beyond the DNS and LES time intervals. For the zero-initial-velocity case, the deposition averaged over the time interval of the LES comparison case ($\tau_p^+ = 200$) is seen to be much lower than for the other (zero-initial-slip) cases, emphasizing that this time interval corresponds to a regime governed primarily by initial conditions.

The convergence of the two model cases is consistent with the predicted (Sec. III.B) insensitivity to initial U values provided that they are not large compared to u'. The two cases converge when both reach a state that is insensitive to initial conditions.

Figure 6 shows a measure of transient relaxation for the model analog of the DNS case ($\tau_p^+ = 50$). Ballistic time is the time until deposition based on a ballistic trajectory, i.e., infinite particle inertia. Inertia can increase or decrease the actual time relative to the ballistic time, but a net decrease occurs only at very early times when deposition is promoted by 'favorable' eddy motions acting on particles initially near a wall. (To simplify the interpretation of this metric, particles that deposit on the wall opposite to the wall encountered ballistically are disregarded.) The relatively slow change of ballistic relative to actual time prior to $t^+ = 150$, corresponding to 3 particle time constants, reflects the deposition of particles whose trajectories retain memory of the initial orientation of the particle velocity vector. The subsequent rapid growth and increased

scatter of this ratio reflects the transition to particle evolution that is insensitive to initial conditions. Fig. 5 indicates that this onset coincides with the attainment of statistically steady deposition for this case. In contrast, the apparent convergence of the two $\tau_p^+ = 200$ cases in Fig. 5 prior to their attainment of statistical steadiness suggests that memory loss precedes the completion of transient relaxation. The overlap of these cases during the late transient is imperfect and may be fortuitous; they unambiguously coincide only when statistical steadiness is attained.

Further detailed investigation would be required to form a complete picture of the process of transition from initial condition sensitivity to insensitivity and the related but distinct process of transient relaxation. The foregoing observations are suggestive of the rich phenomenology of non-equilibrium deposition that remains to be explored.

VI. DISCUSSION

Although the influence of non-equilibration of particle-flow interactions on high-inertia deposition is recognized, experimental methods, models, and numerical simulation tools heretofore applied to this problem have lacked the capability to probe this regime and discern the underlying physics. The heuristic scaling analysis presented here indicates power-law decay of the deposition rate as a function of particle Stokes number τ_p^+ for large τ_p^+. A stochastic model that captures the relevant physics of particle-flow coupling and simulates turbulent channel flow accurately, yet is economical enough for simulation of deposition at very high τ_p^+, is formulated and applied to channel-flow deposition over a wide range τ_p^+. Based on adjustment of one parameter governing particle-flow coupling (in addition to prior adjustment of parameters governing the flow simulation), the model reproduces much of the phenomenology of channel-flow deposition and elucidates the predicted high-inertia scaling.

Specifically, is it shown that the predicted scaling is a far-field asymptote preceded by a transient regime during which deposition is nearly ballistic and therefore insensitive to τ_p^+. The deposition rate during this transient may far exceed the rate during the subsequent statistically steady deposition, so a large majority of particles may deposit during the transient. Typically, the particles that survive the transient are those whose initial trajectories are nearly streamwise so that ballistic motion does not cause early deposition.

The relative contributions of transient and far-field deposition are sensitive to initial conditions. Particles with negligible initial lateral velocity are not subject to the ballistic mechanism, so the deposition rate for particles initialized in this matter is lower during the transient than subsequently.

In published 3D numerical simulations of deposition in the vicinity of the onset of the inertia-moderated regime, the initial particle slip velocity is set equal to zero, a scenario in which the transient deposition rate exceeds the far-field rate and the transient deposition exhibits ballistic scaling (insensitivity to τ_p^+). These simulations are costly, which may be the reason they were not run long enough to reach the far-field regime beyond the initial transient. In addition to this consideration, valid interpretation of the results requires examination of the time-resolved deposition rate, as demonstrated here. The increase of computer capabilities subsequent to the published 3D simulation studies provides the wherewithal for future 3D numerical exploration of the time domain as well as a relevant range of τ_p^+ values. The model results presented here may provide useful guidance for planning these studies and interpreting the results.

Experimental investigation of time-resolved (more precisely, streamwise-resolved because the flow development in experiments is spatial rather than temporal) high-inertia deposition may be more problematic. It is difficult to design an experiment in a confined flow (e.g., a pipe) that is long enough to allow transient relaxation yet is not subject to complications that obscure the quantitative signatures of convergence to statistically steady deposition. The main implication of

the present study with regard to measurements is that the well-known inconsistencies among various reported measurements of high-inertia deposition[2,24] can perhaps be attributed to the sensitivity to initial conditions during the near-field transient, although other contributing factors may be equally if not more significant. The present study indicates that collimation of injected particles would tend to prevent the obscuration of statistically steady deposition by the initial transient.

It is emphasized here that statistically steady deposition does not imply equilibration of particle motions relative to turbulent fluid motions. In fact, it is found that the particle motions are far from equilibrium in the statistically steady deposition regime. It is noted in Sec. III.B that non-equilibrium presents a challenge to closure-type deposition modeling that has not yet been satisfactorily addressed. The present results may aid further developments in this regard by providing guidance concerning the behaviors that should be captured by closure models of deposition.

Graham addresses initial-condition sensitivity, slow relaxation of transients, non-equilibrium effects, and implications concerning the design and interpretation of experiments and numerical simulations, in the context of dispersion in isotropic turbulence.[9] This context allows more precise and detailed analysis than is presented in Sec. III and Appendix B. The present contribution may be viewed as a demonstration, using heuristic analysis and modeling, of the impact of these considerations in the context of deposition in turbulent channel flow.

Thus, the issues addressed here are broader than this particular application. It is anticipated that future application of the analytical and numerical modeling approaches introduced here to other multiphase turbulent flow regimes may provide further useful insight. In this regard, generalization of the present two-phase-flow formulation of ODT to include more elaborate drag laws and multiple scalars, allowing inter-phase couplings such as thermophoresis, should be straightforward. The modeling framework should also accommodate other generalizations such as two-way coupling.

ACKNOWLEDGMENTS

Portions of this work were completed by the first author as his Ph.D. Dissertation in Chemical Engineering at the University of Arizona. This work was also partially supported by the U. S. Department of Energy, Office of Basic Energy Sciences, Division of Chemical Sciences, Geosciences, and Biosciences. Sandia National Laboratories is a multi-program laboratory operated by Sandia Corporation, a Lockheed Martin Company, for the United States Department of Energy under contract DE-AC04-94-AL85000**.**

APPENDIX A: DETAILS OF THE CHANNEL-FLOW SIMULATION

To supplement the turbulence model description in Sec. IV.B, some details of the channel-flow formulation are presented here. Motivation is minimal because it is discussed extensively elsewhere.[13-15,20]

During the T process, the fluid state evolves according to

$$\frac{\partial u_i(y,t)}{\partial t} = \nu \frac{\partial^2 u_i(y,t)}{\partial y^2} - \frac{\delta_{i,1}}{\rho_f}\frac{dp}{dx} \quad , \tag{A1}$$

where (u_1,u_2,u_3) corresponds to (u,v,w) in Sec. IV. The boundary conditions are $u_i(y,t) = 0$ at $y =$ 0 and $2h$.

Apart from particle-eddy interaction (Sec. IV.C), each eddy event consists of two mathematical operations. One is a measure-preserving map representing the fluid displacements. The other is a modification of the velocity profiles in order to account for energy transfers. The combined effect of these operations is denoted

$$u_i(y) \to u_i(f(y)) + c_i K(y). \tag{A2}$$

The fluid at location $f(y)$ is moved to location y by the mapping operation, taken to be the triplet map (see below). This mapping is applied to all fluid properties, including scalars in variable-property flows (not considered here). The additional term $c_i K(y)$, which is only applied to the velocity components, is the ODT analog of pressure-induced energy redistribution among the velocity components, and also accommodates energy exchange with sources and sinks such as gravitational potential energy.

The mapping rule $y \rightarrow y'$ for a triplet map applied to the interval $[y_o, y_o + l]$ is

$$y' = \begin{cases} y_o + \frac{1}{3}(y - y_o) & y_o < y' < y_o + \frac{1}{3} l \\ y_o + \frac{2}{3} l - \frac{1}{3}(y - y_o) & y_o + \frac{1}{3} l < y' < y_o + \frac{2}{3} l \\ y_o + \frac{2}{3} l + \frac{1}{3}(y - y_o) & y_o + \frac{2}{3} l < y' < y_o + l \\ y & \text{otherwise,} \end{cases} \tag{A3}$$

where y' is the post-map y profile. The expressions on the successive lines of Eq. (A3) define the map images denoted y_1', y_2', and y_3', respectively, in Sec. IV.B. $f(y')$ corresponds to the inverse map $y(y')$ implied by Eq. (A3).

In the energy-redistribution term of Eq. (A2), $K(y)$ denotes $y - f(y)$, the displacement of the fluid element mapped to y. It is non-zero only within the eddy interval l and it integrates to zero so that the eddy event does not change the total (y-integrated) momentum of individual velocity components.

The remaining ingredient in the specification of the eddy event is the expression for c_i,

$$c_i = \frac{27}{4l} \left[-u_{i,K} + \operatorname{sgn}(u_{i,K}) \sqrt{\left(\frac{1}{3}\right)\left(u_{1,K}{}^2 + u_{2,K}{}^2 + u_{3,K}{}^2\right)} \right], \tag{A4}$$

where

$$u_{i,K} = l^{-2} \int u_i(f(y)) K(y)\, dy. \tag{A5}$$

This is obtained by requiring that the maximum kinetic energy extractable from the post-map profiles of the respective velocity components should be the same for all velocity components

(equalization of 'available kinetic energy,' the model analog of 'return to isotropy'). The available kinetic energy of u_i is determined by finding the value of b that minimizes the kinetic energy of the profile $u_i + bK(y)$. The difference between the kinetic energies of the u_i and $u_i + bK(y)$ profiles is the available kinetic energy.

Eddy sampling is based on the eddy rate distribution

$$\lambda(y_o,l;t) \equiv \frac{C}{l^2\tau(y_o,l;t)} = \frac{C\nu}{l^4}\sqrt{\left(\frac{1}{3}\right)\left[\left(\frac{u_{1,K}l}{\nu}\right)^2+\left(\frac{u_{2,K}l}{\nu}\right)^2+\left(\frac{u_{3,K}l}{\nu}\right)^2\right]-Z}, \qquad \text{(A6)}$$

where $\lambda(y_o,l;t)\,dy_0\,dl\,dt$ is the probability of an event with parameters in the ranges $[y_o,y_o+dy_o]$ and $[l,l+dl]$, respectively, during $[t,t+dt]$. If the radical in Eq. (A6) has a negative argument, the event rate is taken to be zero. Physically, this represents viscous suppression of the eddy, governed by the parameter Z. C (which scales the rate distribution) and Z are two adjustable parameters of the present ODT formulation. Following Schmidt et al.,[15] they are assigned the values $C = 12.73$ and $Z = 98$ and the constraint $l < h$ (a third empirical assignment) is applied.

Equation (A6) embodies the core physical content of ODT. Its derivation and features are discussed extensively elsewhere,[14] so they are not explained here, but some implications of Eq. (A6) are noted in Appendix B.

APPENDIX B: LOW-INERTIA DEPOSITION

Here, the quadratic dependence of V_d^+ on τ_p^+ indicated by model results at small τ_p^+ values is interpreted. For small τ_p^+, it is assumed that there is a distance $y_w << h$ at which the typical particle velocity V_w is directed toward the wall and is large enough so that $V_w\tau_p > y_w$. This

identifies a wall layer $[0, y_w]$ in which particle inertia is sufficient for the particle to deposit before it comes to rest. (Recall that the lateral fluid velocity is taken to be zero during the T process.)

It is assumed that the particle arrives in the wall layer with velocity V_w through displacement by a particle-eddy interaction. The frequency of such arrivals is estimated.

Equation (A6) implies a lower bound on eddy sizes. The sum of the terms preceding Z in the radical must exceed Z in order for occurrence of the eddy to be allowable. These terms are squares of Reynolds numbers based on a measure of velocity fluctuations; in Eq. (A5), note that a uniform velocity, multiplied by $K(y)$, integrates to zero. For a given level of velocity fluctuations near the wall, this implies that l cannot be arbitrarily small, reflecting viscous dominance near the wall (i.e., the absence of eddies of size y_τ or smaller).

Suppose then that $y_w << l_o$, where l_o is the scale of the smallest eddy events in the vicinity of the wall. This assumption will be verified self-consistently; y_w is found to vanish for vanishing inertia. An eddy that displaces particles to $[0, y_w]$ corresponds to a triplet-mapped interval whose lower bound y_o is in $[0, y_w]$. Therefore particles mapped into this interval arrive at a location that is a distance of at most y_w from y_o. The triplet-map definition then implies that the y range of particles fluxed across $y = y_w$ by the triplet map is of order y_w. This gives a particle flux across y_w that is of order $n\omega y_w$, where n is the particle number density above the wall layer and $\omega(y_w)$ is the frequency of eddies for which $y_o < y_w$. n does not depend on y_w because bulk properties are applicable beyond the wall layer. This is because particles beyond the wall layer require additional eddy interactions before they can deposit, so they are deemed to be spatially homogenized within the bulk flow.

To determine an eddy frequency from the rate distribution given by Eq. (A6), λ is multiplied by an eddy size range and by a y interval corresponding to a range of possible eddy locations. In this case, the range of locations corresponds to the interval $[0, y_w]$ that contains the lower bound y_o of the eddies that contribute to the particle flux across y_w. This contributes a factor y_w

multiplying λ. λ itself is independent of y_w because the variables determining λ vary only on scales much larger than y_w (provided that y_w vanishes with vanishing inertia, as demonstrated shortly). Therefore $\omega(y_w) \sim y_w$, so the particle flux across y_w scales as y_w^2.

y_w is estimated using the relation $y_w \sim V_w \tau_p$. If V_w depends solely on the imputed fluid velocity during the most recent particle-eddy interaction, then it scales as y_w, so this relation is inconsistent because τ_p is the independent variable and therefore cannot be uniquely determined by the analysis.

This inconsistency is analogous to the well-known low-inertia inconsistency of the free-flight model of deposition.[25] Namely, low-inertia deposition cannot be explained based on statistical estimates of fluid motion. This motivates the formulation of models based on idealizations of individual fluid motions, hence a fluctuation picture.[25]

The analog of this consideration in ODT is the particle-eddy-interaction history, which affects particle trajectories because the particle velocity at the inception of each particle-eddy interaction is taken to be its velocity upon completion of its last prior interaction. In ODT, the analog of intense downsweeps deemed to transport particles to the immediate vicinity of the wall[25] is the occurrence of intense bursts of eddy events.[14] Each triplet map increases velocity gradients, thereby intensifying local fluctuations that influence the occurrence of subsequent eddies in that vicinity, as governed by Eq. (A6). This analog of local self-acceleration of the turbulent cascade (i.e., intermittent bursts) reduces eddy time scales and thus increases their imputed velocities during particle-eddy interaction. In conjunction with the history effect, the effect of these bursts on particle motion is analogous to the effect of downsweeps.

Cleaver and Yates used a simple analytical model of downsweeps to estimate deposition rates.[25] There is no obvious method for analyzing burst statistics in ODT other than to collect and analyze simulation data. Nevertheless, the low-inertia deposition results can be interpreted

straightforwardly by making a simple assumption and comparing the predicted outcome to the ODT deposition results.

In the limit of vanishing inertia, it is reasonable to suppose that the non-vanishing history contribution to V_w depends neither on y_w nor τ_p. Then the relation $y_w \sim V_w \tau_p$ implies $y_w \sim \tau_p$ in this limit, so the particle flux across y_w scales as τ_p^2. Expressed in wall normalization, this yields quadratic dependence of V_d^+ on τ_p^+, consistent with the model tendency at low inertia. The absence of Re sensitivity at low inertia (Fig. 3) indicates that there is no discernible dependence of V_w on outer variables such as u_b.

In the simulations for $\tau_p^+ \leq 50$, particle diameter is based on particle density 713 times the fluid density. To verify that finite particle size does not explain the observed quadratic scaling, note that particle radius r scales as $(\tau_p^+)^{1/2}$ according to Eq. (13). Assume that deposition occurs when $y_w = r$. The particle flux across $y_w = r$ scales as r^2 and therefore as τ_p^+. This yields linear rather than quadratic dependence of V_d^+ on τ_p^+, so it does not explain the computed model behavior. As τ_p^+ is reduced with particle density held fixed, an eventual crossover to this linear dependence is anticipated.

The model of Cleaver and Yates predicts a different functional dependence at low inertia than indicated by ODT. Neither model is expected to provide a quantitatively accurate representation of the flow fluctuations that govern this regime. ODT has the advantage that it can incorporate more realistic drag laws than considered here, so a quantitative test of its accuracy in comparison to the low-inertia DNS results in Fig. 2 can be performed in the future.

REFERENCES

[1] A. Soldati, "Particles turbulence interactions in boundary layers," Z. Angew. Math. Mech. **85**, 683 (2005).

[2] J. Young and A. Leeming, "A theory of particle deposition in turbulent pipe flow," J. Fluid Mech. **340**, 129 (1997).

[3] M. Shin and J. W. Lee, "Memory effect in the Eulerian particle deposition in a fully developed turbulent channel flow," J. Aerosol Sci. **32**, 675 (2001).

[4] M. Shin, D. S. Kim, and J. W. Lee, "Deposition of inertia-dominated particles inside a turbulent boundary layer," Int. J. Multiphase Flow **29**, 893 (2003).

[5] B. Y. Liu, and J. K. Agarwal, "Experimental observation of aerosol deposition in turbulent flow," J. Aerosol Sci. **5**, 145 (1974).

[6] W. S. J. Uijttewaal and R. V. A. Oliemans, "Particle dispersion and deposition in direct numerical and large eddy simulations of vertical pipe flows," Phys. Fluids **8**, 2590 (1996).

[7] M. Chen and J. B. McLaughlin, "A new correlation for the aerosol deposition rate in vertical ducts," J. Colloid Interface Sci. **169**, 437 (1995).

[8] Q. Wang, K. D. Squires, M. Chen, and J. B. McLaughlin, "On the role of the lift force in turbulence simulations of particle deposition," Int. J. Multiphase Flow **23**, 749 (1996).

[9] D. I. Graham, "Development of particle dispersion characteristics from arbitrary initial conditions in isotropic turbulence," J. Fluid Mech. **501**, 149 (2004).

[10] D. B. DeGraaff, and J. K. Eaton, "Reynolds-number scaling of the flat-plate turbulent boundary layer," J. Fluid Mech. **422**, 319 (2000).

[11] S. Hoyas, and J. Jimenez, "Scaling of the velocity fluctuations in turbulent channels up to Re-tau = 2003," Phys. Fluids **18**, 11702 (2006).

[12] G. Gioia, and P. Chakraborty, "Turbulent friction in rough pipes and the energy spectrum of the phenomenological theory," Phys. Rev. Lett. **96**, 44502 (2006).

[13] A. R. Kerstein, "One-dimensional turbulence: model formulation and application to homogeneous turbulence, shear flows, and buoyant stratified flows," J. Fluid Mech. **392**, 277 (1999).

[14] A. R. Kerstein, W. T. Ashurst, V. Nilsen, and S. E. Wunsch, "One-dimensional turbulence: Vector formulation and application to free shear flows," J. Fluid Mech. **447**, 85 (2001).

[15] R. C. Schmidt, A. R. Kerstein, S. E. Wunsch, and V. Nilsen, "Near-wall LES closure based on One-Dimensional Turbulence modeling," J. Comp. Phys. **186**, 317 (2003).

[16] A. R. Kerstein, "Linear-eddy modeling of turbulent transport. Part V: Geometry of scalar interfaces," Phys. Fluids A **3**, 1110 (1991).

[17] J. R. Schmidt, J. O. L. Wendt, and A. R. Kerstein, "Prediction of particle laden turbulent channel flow using One Dimensional Turbulence." Proceedings of the IUTAM Symposium on Computational Approaches to Disperse Multiphase Flow, Argonne National Lab. Argonne, IL October, (2004).

[18] D. I. Graham and P. W. James, "Turbulent dispersion of particles using eddy interaction models," Int. J. Multiphase Flow **22**, 157 (1996).

[19] A. R. Kerstein and S. K. Krueger, "Clustering of randomly advected low-inertia particles: A solvable model," Phys. Rev. E **73**, 25302 (2006).

[20] J. R. Schmidt, "Stochastic models for the prediction of individual particle trajectories in One Dimensional Turbulence flows," PhD Dissertation, Department of Chemical and Environmental Engineering, The Univ. of Arizona (2004).

[21] P. N. Rowe, "The drag coefficient of a sphere," Trans. Inst. Chem. Eng. **39**, 175 (1961).

[22] J. B. McLaughlin, "Aerosol particle deposition in numerically simulated channel flow," Phys. Fluids A **1**, 1211 (1989).

[23] R. A. Farmer, "Liquid droplet trajectories in two phase flow," PhD thesis, MIT (1969).

[24] D. D. McCoy and T. J. Hanratty, "Rate of deposition of droplets in annular two-phase flow," Int. J. Multiphase Flow **3**, 319 (1977).

[25] J. W. Cleaver, and B. Yates, "A sub layer model for the deposition of particles from a turbulent flow," Chem. Eng. Sci. **30**, 983 (1975).

LIST OF CAPTIONS

FIG. 1. Dependence of normalized particle deposition rate V_d^+ on normalized Stokes number τ_p^+ in turbulent channel flow, using Stokes drag. ○, ODT for $\beta = 0.3$, $\mathrm{Re}_\tau = 180$; ●, DNS[22] for $\mathrm{Re}_\tau = 125$.

FIG. 2. (Color online) Comparison of ODT deposition rates, for the same conditions as Fig. 1 data, to simulations and measurements. Stars, ODT; □, DNS;[7] + and ×, measurements[5] for flow Reynolds numbers 10,000 and 50,000, respectively; ●, measurements.[23] Line slopes: – – – –, +2; — · · —, -2/3; ———, -1/2.

FIG. 3. (Color online) ODT results of Fig. 2 in the format of that figure, and additional ODT results for $\mathrm{Re}_\tau = 640$ (□) and 1200 (◊). Line slopes: – – – –, +2; — · · —, -2/3. Otherwise, the same symbol definitions as in Fig. 2.

FIG. 4. (Color online) A portion of the data of Fig. 2, and additional results: Filled stars, transient ODT; Δ, LES.[24] Otherwise, the same symbol definitions as in Fig. 2.

FIG. 5. (Color online) For ODT at $\mathrm{Re}_\tau = 180$ using corrected drag, dependence of deposition rate on elapsed time in wall units for $\tau_p^+ = 50$ (+), 100 (×), and 200 (□). ○, same as the ODT $\tau_p^+ = 200$ case but with zero-particle-velocity initial condition and particle initial spatial distribution as described in the main text; — · —, average for this case over the time interval spanned by the line. Other lines are also averages over the spanned time interval: ———, DNS[7] for $\tau_p^+ = 50$; – – – – and — · · —, LES for $\tau_p^+ = 100$ and 200, respectively.[8]

FIG. 6. For the ODT case denoted by + in Fig. 5, ratio of actual to ballistic (infinite-inertia) particle deposition time, conditioned on both depositions occurring on the same wall. This ratio is shown as a function of actual deposition time in wall units.

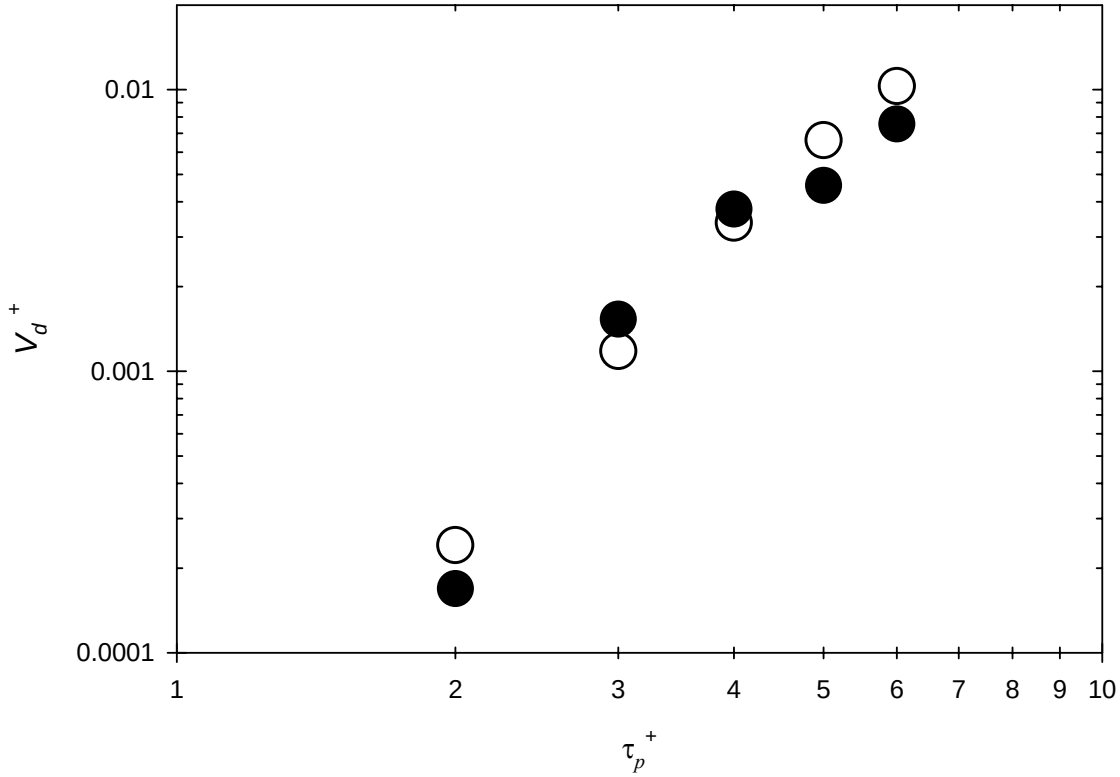

Figure 1.

J.R. Schmidt, J.O.L. Wendt, and A.R. Kerstein

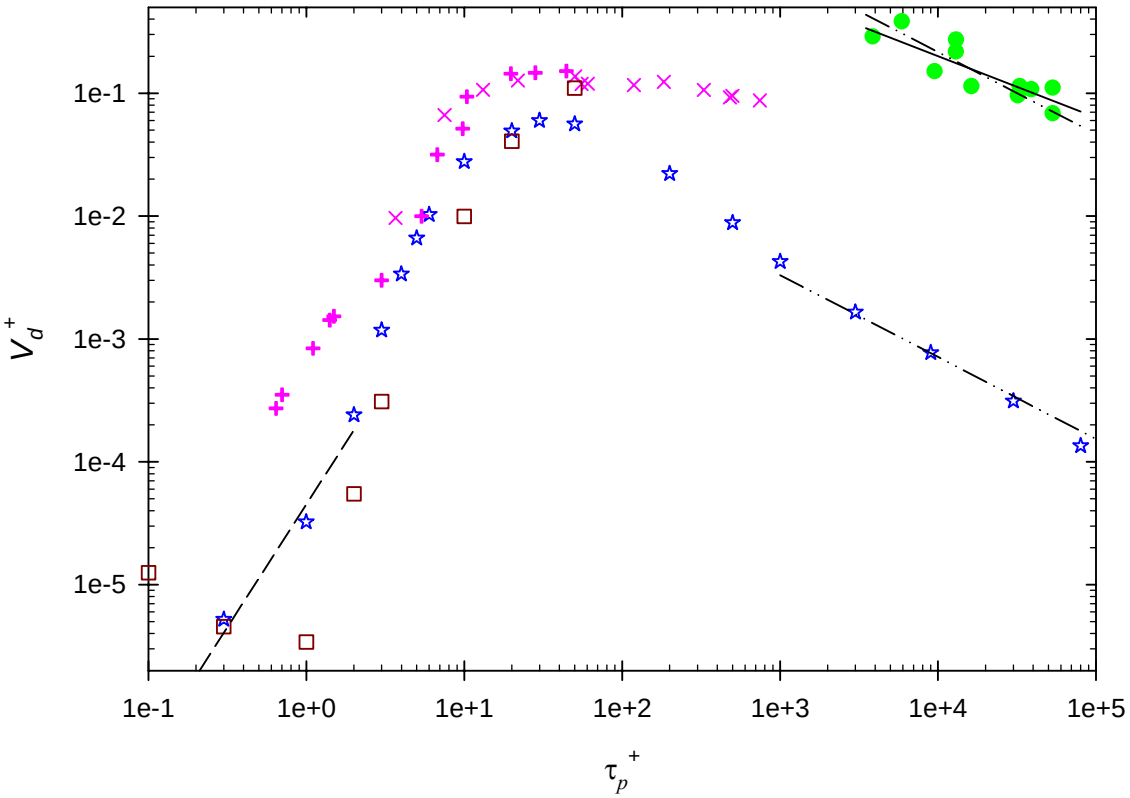

Figure 2.

J.R. Schmidt, J.O.L. Wendt, and A.R. Kerstein

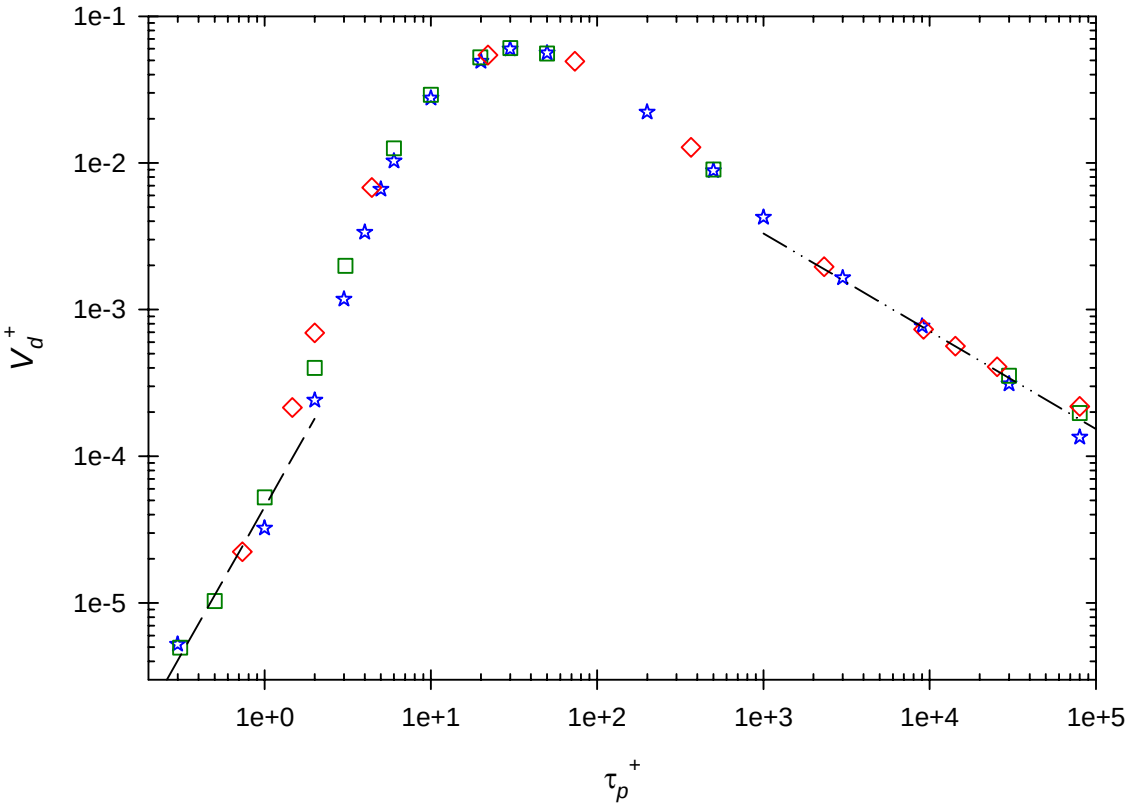

Figure 3.

J.R. Schmidt, J.O.L. Wendt, and A.R. Kerstein

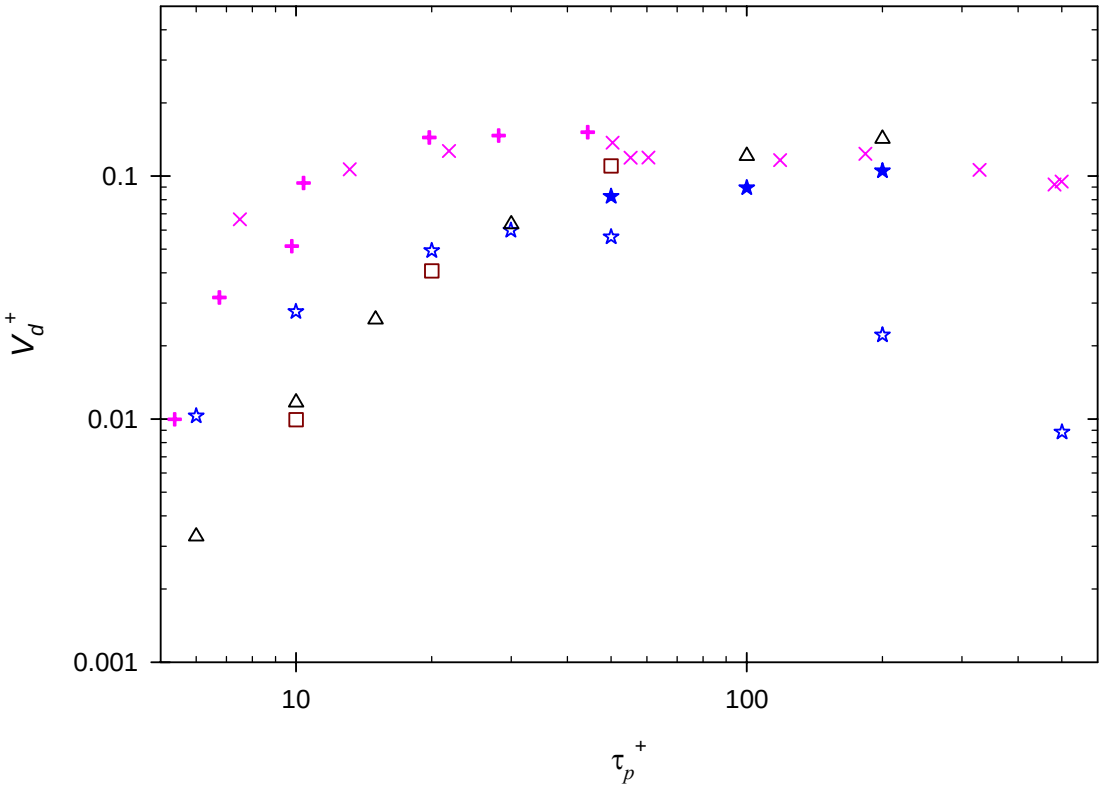

Figure 4.

J.R. Schmidt, J.O.L. Wendt, and A.R. Kerstein

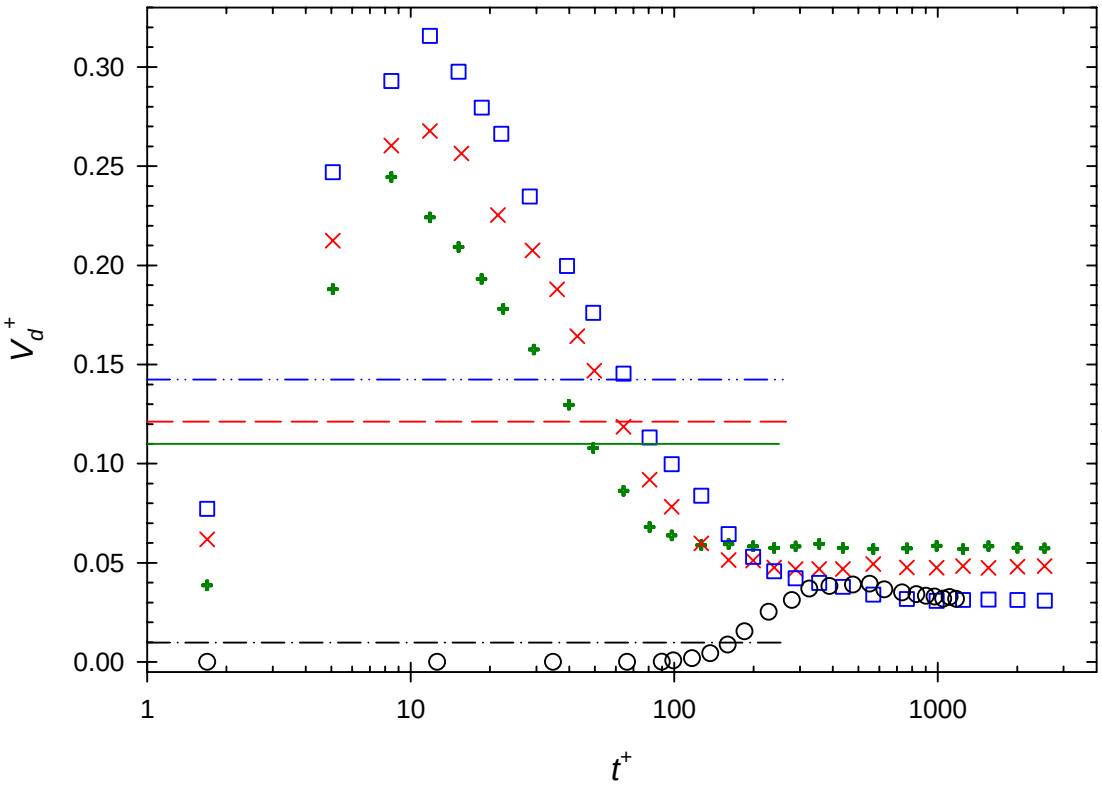

Figure 5.

J.R. Schmidt, J.O.L. Wendt, and A.R. Kerstein

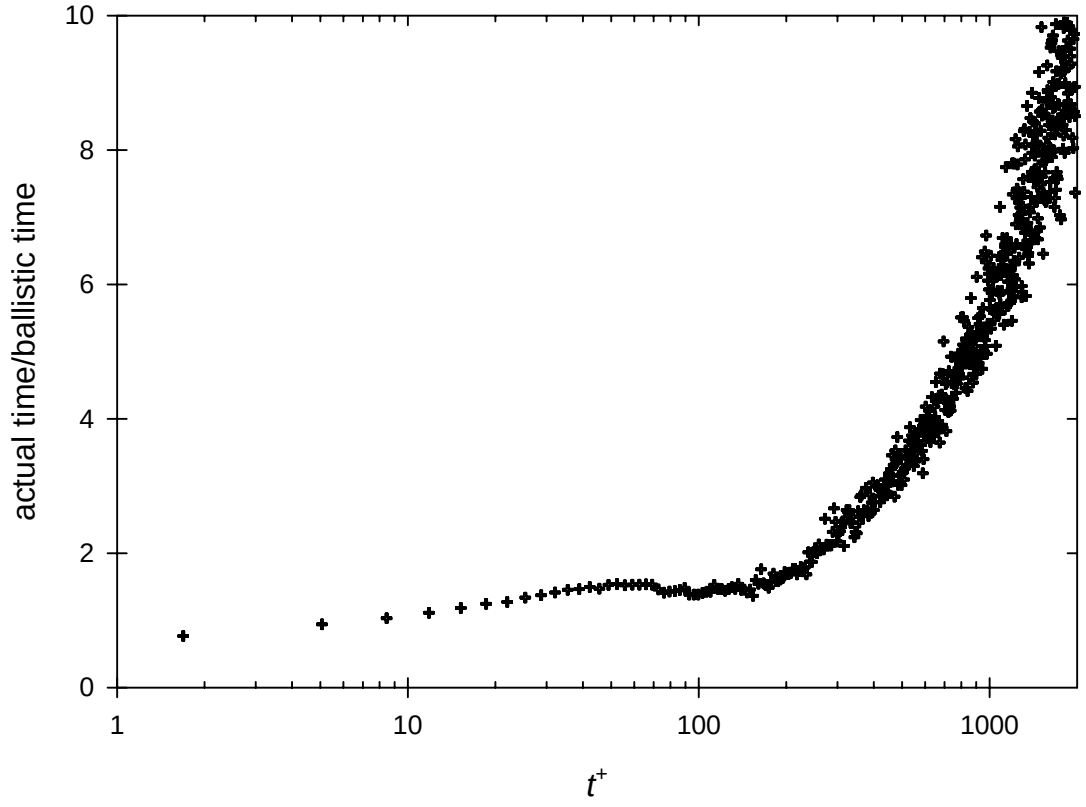

Figure 6.

J.R. Schmidt, J.O.L. Wendt, and A.R. Kerstein